ACS OMEGA

http://pubs.acs.org/journal/acsodf

Article

Resistive Water Level Sensors Based on AgNWs/PEDOT:PSS-*g*-PEGME Hybrid Film for Agricultural Monitoring Systems

Seungho Baek,[#] Jung Joon Lee,[#] Jonghwan Shin, Jung Ho Kim, Seongin Hong,[*] and Sunkook Kim[*]

Cite This: *ACS Omega* 2022, 7, 15459−15466

Read Online

ACCESS | Metrics & More | Article Recommendations | Supporting Information

ABSTRACT: Recently, an agricultural monitoring system using the Internet of Things has been developed to realize smart farming. The high performance of various sensors in agricultural monitoring systems is essential for smart farming to automatically monitor and control agricultural environmental conditions such as temperature and water level. In this study, we propose resistive water level sensors based on an AgNWs/PEDOT:PSS-*g*-PEGME hybrid structure to improve the already high conductivity and water stability of PEDOT:PSS. After spin-coating the AgNWs/PEDOT:PSS-*g*-PEGME hybrid film, a laser treatment method successfully patterns the resistive water level sensor with areas of higher resistance. When water contacts the sensor, the variation in resistance caused by the water level changes the current flow of the sensor, allowing it to be used to detect the water level. Finally, we develop a water level sensor module as a component of the agricultural monitoring system by connecting the sensor to a microcontroller for water level monitoring in real time. The proposed water level sensors may be a new solution for detecting water levels in agricultural monitoring systems.

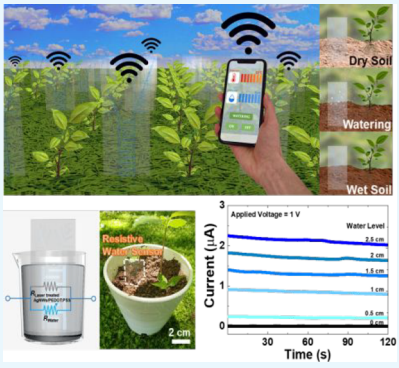

INTRODUCTION

With the advent of the Internet of Things (IoT), an agricultural monitoring system for smart farming has been developed and utilized, enabling remote monitoring and control of agricultural environmental conditions such as temperature, humidity, light, and water level.[1−8] Accordingly, the agricultural monitoring systems for smart farming comprise various sensors, such as temperature and humidity sensors, light detectors, pH sensors, etc.[9−11] The accurate detection of water level is crucial for automatically and optimally watering agricultural crops. Resistive type water level sensors are suitable for agricultural monitoring systems owing to their simplicity, ease of operation, and low manufacturing cost compared with those of other types of water level sensors, such as ultrasonic, magnetic float, and radar level sensors.[12−15] When a plant is watered, the water comes in contact with the resistive water level sensor next to the plant, resulting in the detection of water level by the reduced the resistance of the water level sensor.

Recently, poly(3,4-ethylenedioxythiophene):poly(styrenesulfonate) (PEDOT:PSS) has been considered as a promising electrode material owing to its high conductivity, transparency, flexibility, and solution processability.[16−20] However, the limitation of PEDOT:PSS is that electrodes are relatively difficult to integrate into circuits and desired patterns once coated using the solution processes. The laser treatment method can easily achieve the required patterning of PEDOT:PSS, as discussed in our previous report.[15] Moreover, improved conductivity and water stability of PEDOT:PSS are still required for water level sensors compared with conventional metals.[21,22] Hybridizing PEDOT:PSS with other materials such as metal nanowires (NWs) and poly(ethylene glycol) methyl ether (PEGME) may result in higher water stability and conductivity.

In this study, we introduce resistive water level sensors based on an AgNWs/PEDOT:PSS-*g*-PEGME hybrid film for agricultural monitoring systems. To overcome the limitations of ordinary PEDOT:PSS, we hybridized PEDOT:PSS-*g*-PEGME with AgNWs, resulting in reduced solubility and improved conductivity. The AgNWs/PEDOT:PSS-*g*-PEGME hybrid film was successfully deposited onto the PET film by sequentially and repeatedly spin-coating the AgNWs and the fabricated PEDOT:PSS-*g*-PEGME solution, followed by individual annealing at each step. The infrared laser treatment method patterns the hybrid film with two separated patterns of electrodes. The laser-treated region between the two groups of electrodes exhibits a relatively lower conductivity (i.e., higher resistance), demonstrated by scanning electron microscopy (SEM) and X-ray photoelectron spectroscopy (XPS) analysis,

Received: January 2, 2022
Accepted: February 24, 2022
Published: April 26, 2022

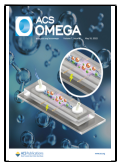

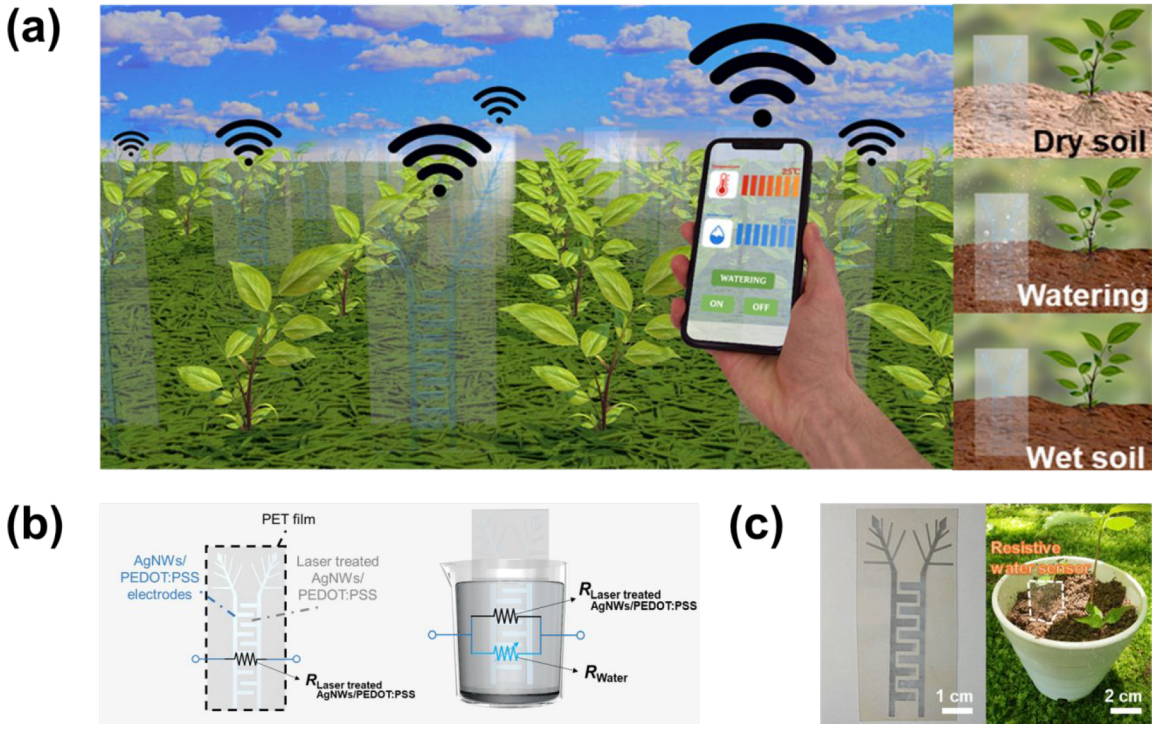

Figure 1. Depictions of the resistive water level sensor. (a) Graphic showing the application of the resistive water level sensor in an agricultural monitoring system. (b) Diagram of the resistive water level sensor and equivalent circuit. (c) Photographs of the resistive water level sensor on PET film and the sensor in a flowerpot beside a plant.

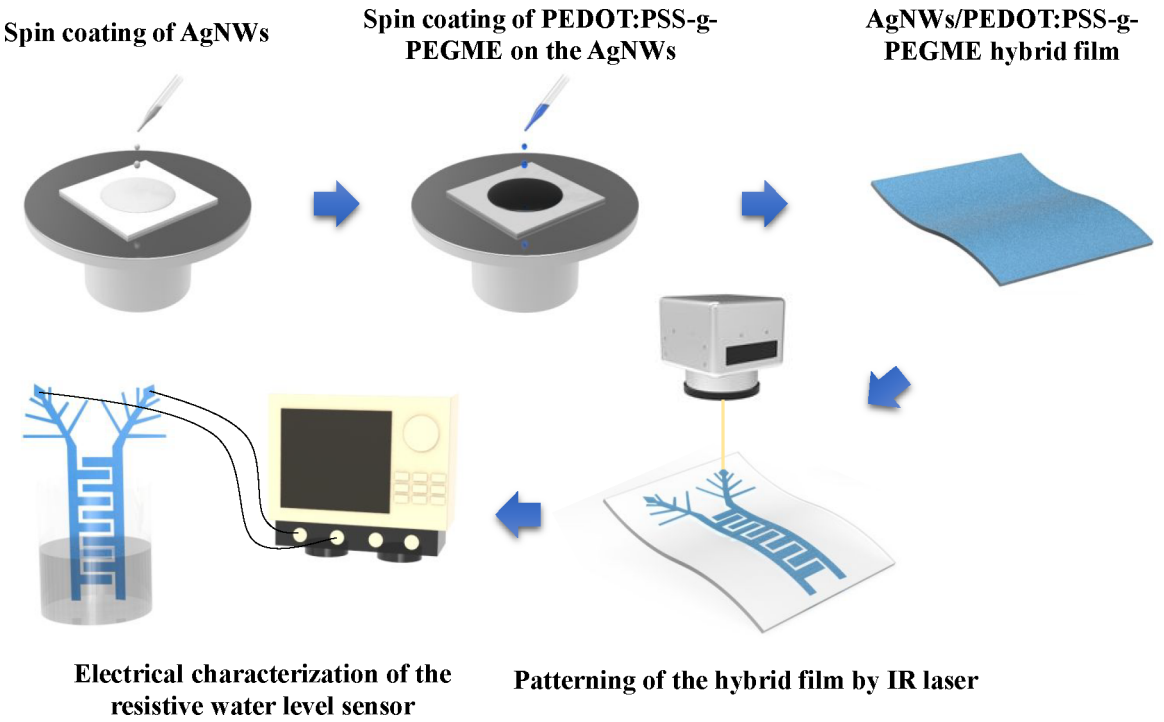

Figure 2. Schematic of the fabrication process of the resistive water level sensor.

as well as the electrical properties. The electrical characteristics of the resistive water level sensor based on the AgNWs/PEDOT:PSS-*g*-PEGME hybrid film were investigated under various water levels. It was found that the current increased as the water level increased due to the change in the resistance. Conductivity and stability of this sensor based on an AgNWs/PEDOT:PSS-*g*-PEGME hybrid film were higher than our previous report, making it applicable to agricultural applications. Finally, we implemented a water level sensor module for the agricultural monitoring system by connecting the sensor and microcontroller (Arduino Uno), resulting in accurate water level detection in real time. We believe that the proposed water level sensors provide a new technique for detecting accurate water levels for agricultural monitoring systems.

https://doi.org/10.1021/acsomega.2c00017
ACS Omega 2022, 7, 15459−15466

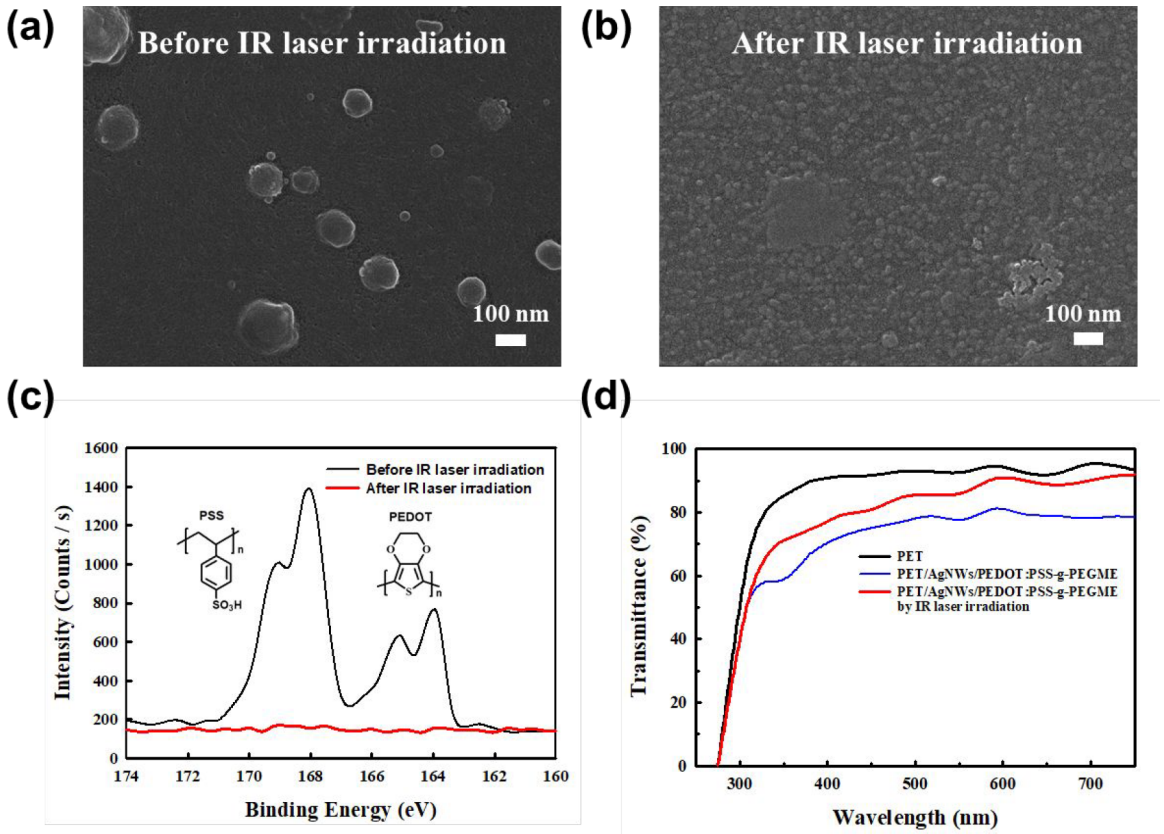

Figure 3. Spectroscopic analysis of the AgNWs/PEDOT:PSS-*g*-PEGME hybrid film on PET before and after IR laser irradiation. SEM images (a) before and (b) after IR laser irradiation. (c) XPS spectrum of sulfur 2p. (d) Optical transmittance.

RESULTS AND DISCUSSION

Figure 1a depicts a conceptual 3D image of the water level sensor for the agricultural monitoring system. Water level sensors are placed next to agricultural crops for the real-time monitoring of the water level. When humidity sensors in an agricultural monitoring system detect crops that need water, the farmer waters the crops using a smartphone. The water level sensor notifies the farmer of the water level being applied to the soil in real time while watering the crop, as depicted on the right side of Figure 1a. Figure 1b illustrates the specific water level sensor structure comprising two AgNWs/PEDOT:PSS electrodes and a laser-treated AgNWs/PEDOT:PSS region as the resistive component. The water level detection of the sensor relies on the decrease in resistance of the sensor with increasing water level, as discussed in our previous report.[15] Once the water comes in contact with the surface of the sensor, the resistance component can be calculated using $R_{\text{laser treated AgNWs/PEDOT:PSS}}$ and R_{water} in parallel (i.e., $R_{\text{total}} = R_{\text{laser treated AgNWs/PEDOT:PSS}} \parallel R_{\text{water}} = (R_{\text{laser treated AgNWs/PEDOT:PSS}} \times R_{\text{water}})/(R_{\text{Llaser treated AgNWs/PEDOT:PSS}} + R_{\text{water}})$). R_{water} decreases with the increasing water level, resulting in a decrease in R_{total}. Figure 1c shows both the photographs of the fabricated water level sensor created using the laser treatment method and the sensor located next to a plant. The details of the fabrication process of the water level sensor are depicted in Figure 2 and described in the Methods.

Figure 2 illustrates a schematic of the fabrication process for the resistive water level sensor. AgNWs are first coated on the top of the PET, and a PEDOT:PSS-*g*-PEGME copolymer was overcoated on the AgNWs to fabricate the hybrid film. The thickness of the hybrid film was 147 nm. The PEDOT:PSS-*g*-PEGME copolymer was applied to utilize PEDOT:PSS as a water level sensor. Ordinary PEDOT:PSS films easily dissolve because the sulfonic acid group of PSS dissolves in water with SO_3^- and H^+. To prevent this, a PEDOT:PSS-*g*-PEGME copolymer, which is water resistant through an esterification reaction between PEDOT:PSS and PEGME, is introduced in this study. The atmospheric stability and water resistance of the PEDOT:PSS-*g*-PEGME copolymer have been demonstrated in previous studies.[15,21] PEDOT:PSS-*g*-PEGME is water resistant, maintaining its characteristics such as conductivity, transmittance, and flexibility in water compared to those of ordinary PEDOT:PSS. Therefore, PEDOT:PSS-*g*-PEGME is a highly suitable conducting copolymer for water level sensors. For lower resistance films, PEDOT:PSS-*g*-PEGME was combined with AgNWs in a layer-by-layer form to further improve the performance of the water level sensor. IR lasers are utilized for patterning the hybrid film to create the water level sensor as they are simple and easy to use, can quickly handle large areas, and do not react with the substrate PET, allowing only the coated hybrid film to be affected.[23−25] The laser beam has a diameter of 20 μm and a wavelength of 1054 nm. Finally, the water level sensor can detect the height of the water through both its ends.

Before and after the IR laser irradiation, the morphology of the AgNWs/PEDOT:PSS-*g*-PEGME hybrid film was analyzed using SEM, as shown in Figure 3a,b. Particles measuring tens to hundreds of nanometers in diameter were split into many smaller particles of approximately 20−30 nm diameter after the IR laser irradiation. This suggests that the particles reacted under the IR laser. EDX was used to analyze the patterning of the IR lasers for the hybrid film. After the IR irradiation, the Ag

https://doi.org/10.1021/acsomega.2c00017
ACS Omega 2022, 7, 15459−15466

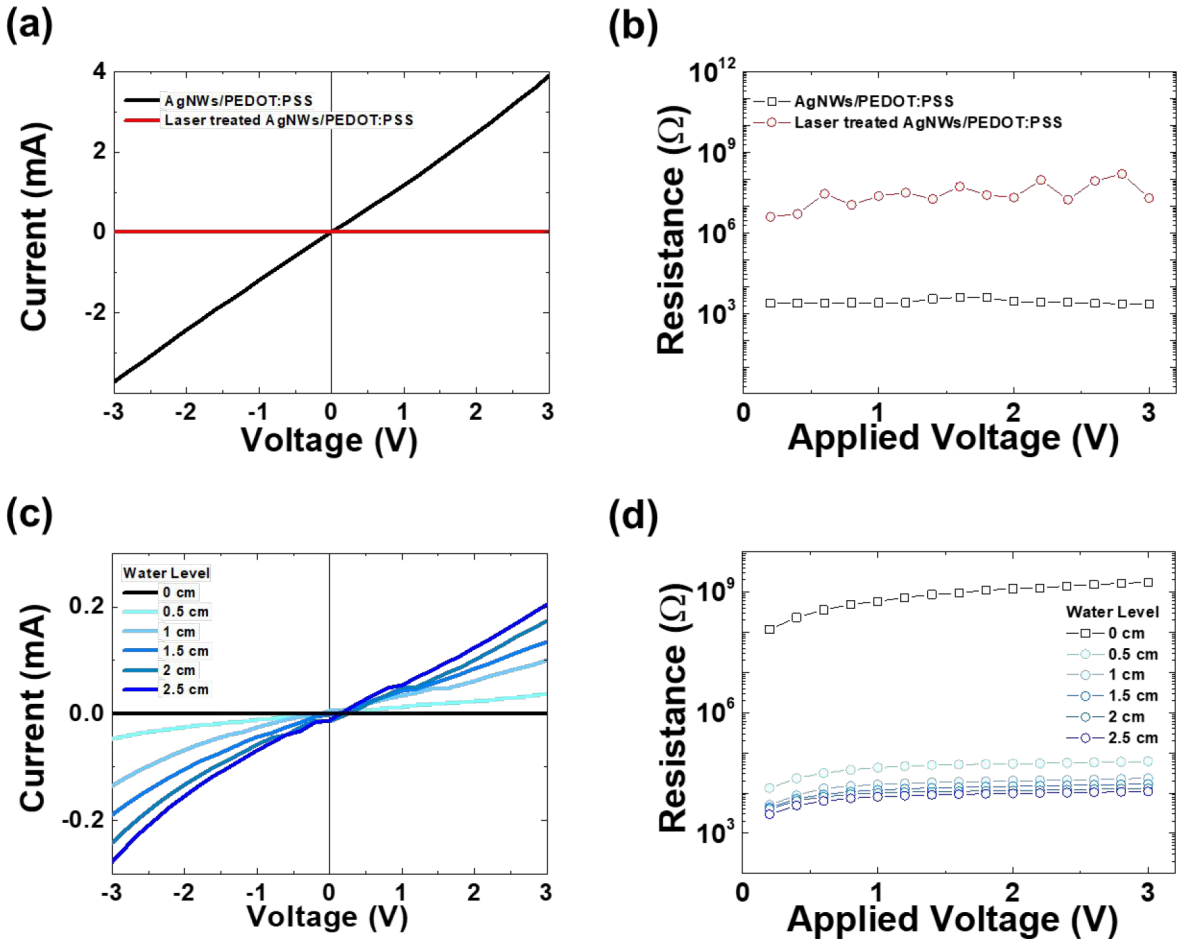

Figure 4. Electrical characteristics of the resistive water level sensor. (a) $I-V$ curves of normal and laser-treated AgNWs/PEDOT:PSS regions. (b) Resistance of AgNWs/PEDOT:PSS copolymer and laser-treated AgNWs/PEDOT:PSS. (c) $I-V$ curves of the resistive water level sensor dipped in water levels from 0 to 2.5 cm. (d) Resistance of the resistive water level sensor with increasing water level from 0 to 2.5 cm.

element was completely removed, decreasing its content from 0.2% to 0%, as shown in Table S1 and Figure S1a,b. The S content of PEDOT:PSS decreased by 94.5%, from 0.73% to 0.04%. XPS analysis was performed to confirm more accurately the patterning of PEDOT:PSS by through laser irradiation (Figure 3c). The binding energy of 163−167 eV corresponds to the S element of PEDOT, and the binding energy of 167−171 eV corresponds to the S element of PSS in the XPS analysis.[26,27] After IR irradiation, the PEDOT:PSS peak disappeared, indicating that the IR laser with a wavelength of 1054 nm is also effective in patterning PEDOT:PSS as well as Ag. Using EDX, the remaining 0.04% of S after the IR irradiation was estimated to be the remaining residual after the reaction with the IR laser (Figure S1 and Table S1). A pattern on the hybrid film also affects the transmittance. As depicted in Figure 3d, the transmittance of the hybrid film after IR laser irradiation increased by 7.9% from 78.4% to 86.3% at 550 nm. This is attributed to the increased transmittance of the hybrid film by the IR laser irradiation.

Figure 4a depicts the electrical characteristics of the AgNWs/PEDOT:PSS region and laser-treated AgNWs/PEDOT:PSS region. The AgNWs/PEDOT:PSS region exhibits ohmic resistor behaviors with high conductivity, whereas the laser-treated AgNWs/PEDOT:PSS region demonstrates significantly low conductivity owing to the reduction in conductive elements by the laser treatment. Figure 4b depicts the resistances of these regions calculated from Figure 4a using the equation $R = V/I$, where R is the resistance, V is the applied voltage, and I is the current. The calculated resistance of the laser-treated AgNWs/PEDOT:PSS region ($\sim 10^7$ Ω) was 10^4 times higher than that of the AgNWs/PEDOT:PSS region ($\sim 10^3$ Ω), indicating that the laser treatment removed almost all the conductive elements such as Ag and S. Figure 4c depicts the electrical characteristics of the water level sensor under various water levels measured at both the AgNWs/PEDOT:PSS region as the electrodes and the laser-treated AgNWs/PEDOT:PSS region as the resistive component. The current gradually increased with increasing water levels from 0 to 2.5 cm. When the water came in contact with the surface of the sensor and increased the water level, the resistance between the two AgNWs/PEDOT:PSS electrodes (i.e., the laser-treated AgNWs/PEDOT:PSS region) was reduced, resulting in a current increase of the sensor. Therefore, the current variation caused by the watering can be used to measure water level (see Figure 6). The extracted resistance of the water level sensor decreased sequentially as the water level increased in 0.5 cm steps (Figure 4d). The laser-treated AgNWs/PEDOT:PSS region acts as resistive component ($R_{\text{laser treated AgNWs}/\text{PEDOT:PSS}}$). When water comes into the surface of the sensor, a variable resistance (R_{water}) that changes according to the water level is created. Therefore, the sensor in water has two parallel resistors ($R_{\text{laser treated AgNWs}/\text{PEDOT:PSS}}$ ||

https://doi.org/10.1021/acsomega.2c00017
ACS Omega 2022, 7, 15459−15466

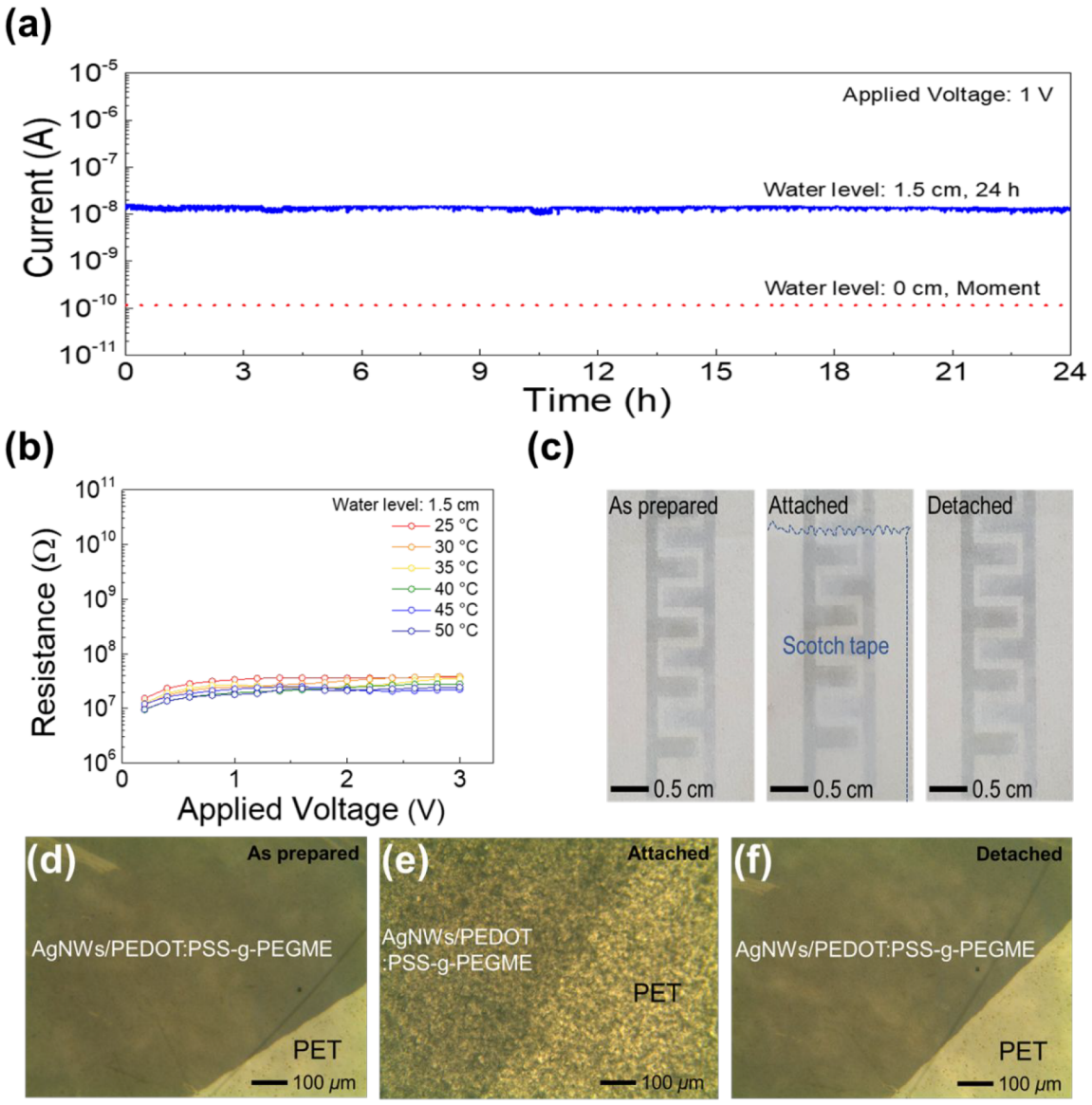

Figure 5. Stability tests of the resistive water level sensor. (a) Detection stability test of the sensor under a water level of 1.5 cm for 24 h. (b) Resistance of the sensor with a water level of 1.5 cm under various temperatures (25−50 °C, +10 °C steps). (c) Photograph of the resistive water level sensor during the Scotch tape test. The test was performed by attaching and then detaching Scotch tape on the surface of the sensor. Optical microscope images of the resistive water level sensor (d) as prepared, (e) attached with Scotch tape, and (f) detached with Scotch tape.

R_{water}; see Figure 1b), which is expressed as the equation of $R_{total} = (R_{laser\ treated\ AgNWs/PEDOT:PSS} \times R_{water})/(R_{laser\ treated\ AgNWs/PEDOT:PSS} + R_{water})$. As the water level rises, R_{water} decreases, and eventually R_{total} becomes smaller, resulting in current changes according to the water level.

Figure 5 shows the stability tests of the sensor for agricultural applications, which were conducted by using various parameters (time for long-term detection, temperature by sunlight, and surface robustness against soil and mud). Current−time characteristics of the resistive water level sensor under a water level of 1.5 cm for 24 h exhibit great detection stability, as shown in Figure 5a. The resistances of sensor were measured under various temperatures to investigate temperature stability of the sensor. The slight resistance change of the resistive water level sensor in temperature increasing as shown in Figure 5b, which is negligible in measuring the water level for agricultural applications. Next, we performed an adhesion test through the attaching Scotch tape (3M, Model No. 801) on the surface of the resistive water level sensor as shown in Figure 5c. Figure 5 panels d−f show optical microscope images of the AgNWs/PEDOT:PSS-*g*-PEMGE film on the substrate before and after the Scotch tape test, indicating great adhesion on the substrate. The enhanced stability performance of the sensor compared to our previous report[15] made it applicable to agricultural monitoring system.

To investigate the real-time monitoring performance of the water level sensor, current−time curves were measured for 120 s under water levels of 0−2.5 cm in intervals of 0.5 cm at an applied voltage of 1 V, as depicted in Figure 6a. The current at each water level was maintained until 120 s of equal performance passes. The current variation ratio was calculated using the equation $\Delta I/I_0 = (I_w - I_0)/I_0$, where I_0 and I_w denote the initial and final current for each water level, respectively. This clearly indicates the relationship between $\Delta I/I_0$ and the water level, as shown in Figure 6b. The average current values linearly increased with increasing water level, and their

https://doi.org/10.1021/acsomega.2c00017
ACS Omega 2022, 7, 15459−15466

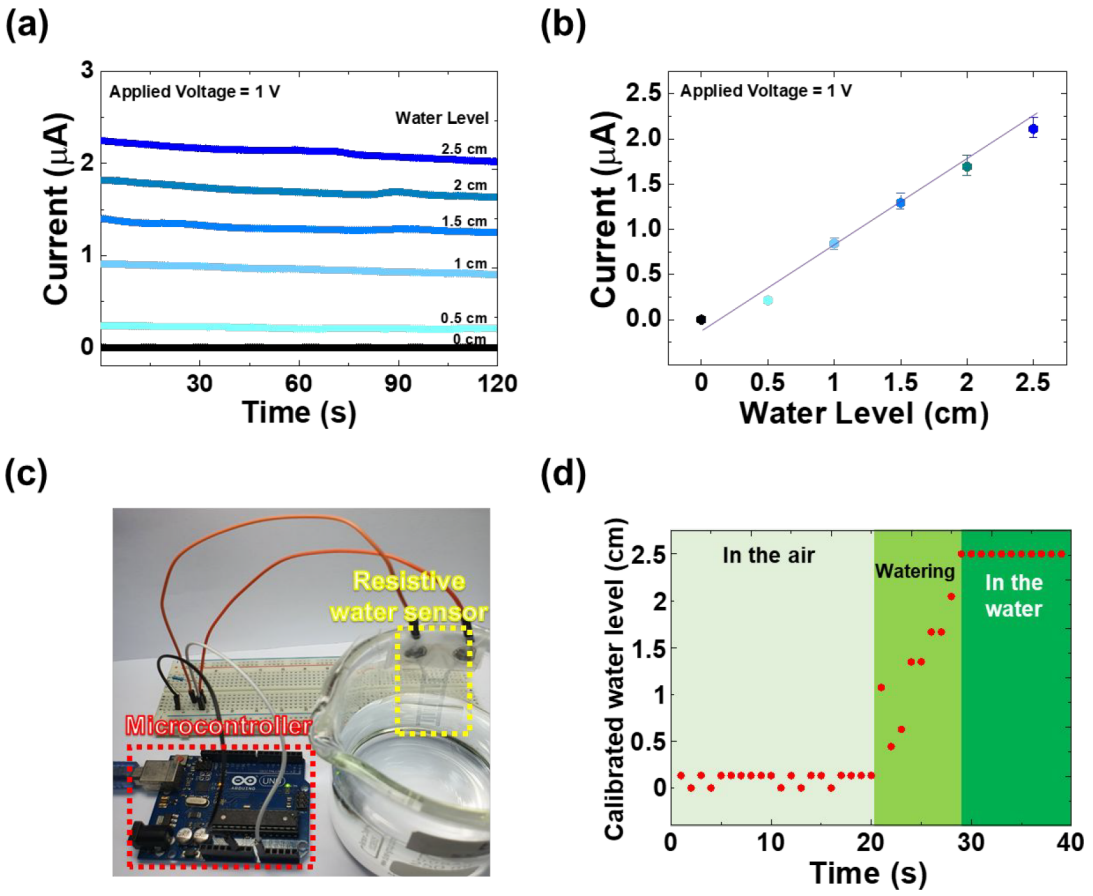

Figure 6. Real-time measurement of the water level using the resistive water level sensor. (a) Time−current curves of the resistive water level sensor for 120 s at 1 V applied voltage. (b) Statistical analysis of the current with varying water levels at 1 V applied voltage. (c) Photograph of the resistive water level sensor connected to a microcontroller. (d) Response of water level sensor module to the resistive water level sensor under water level increments (dipping rate ∼0.8 cm/s up to 2.5 cm).

coefficient of variation remained below 6%, indicating a high sensor stability. Figure 6c depicts a water level sensor module connected to a water level sensor fabricated on the AgNWs/PEDOT:PSS-*g*-PEGME hybrid film with a microcontroller (Arduino Uno) to demonstrate the real-time monitoring of agricultural systems. The detection of the water level sensor module in real time was performed while the sensor was inserted into the water with a manual dipping speed of ∼0.8 cm/s from 0 to 2.5 cm. Figure 6d depicts the calibrated water level−time curves, which in turn demonstrate excellent water level sensing in real time. These results indicate that our study provides a novel approach for agricultural monitoring systems in smart farming.

CONCLUSION

In this study, resistive water level sensors were developed on the basis of a AgNWs/PEDOT:PSS-*g*-PEGME hybrid film for agricultural monitoring systems. Hybridization of AgNWs and PEGME into PEDOT:PSS improved the conductivity and water stability, respectively. Laser treatment enabled the fabrication of a resistive water level sensor comprising two electrode regions and between them a laser-treated region with high resistance. When the sensor next to the crop was in contact with the water, the variations in the resistance detected with the water level allowed an accurate detection of the water level. Thus, the water level module connected to the sensor and microcontroller for real-time monitoring was successful. We believe that the proposed water level sensor may provide a novel promising approach for agricultural monitoring systems in smart farming.

METHODS

Materials. Poly(3,4-ethylenedioxythiophene) (PEDOT:PSS, Clevios PH 1000) solution and silver nanowires (AgNWs) solution were purchased from Heraeus Ltd. and C3Nano Inc., respectively. Poly(ethylene glycol) methyl ether (PEGME, Average Mn 550) and dimethyl sulfoxide (DMSO) were obtained from Sigma-Aldrich. Capstone fs-30 (wetting agent) was sourced from Chemours Co. All materials were used without further purification.

Fabrication of Water Level Sensor Using AgNWs/PEDOT:PSS-*g*-PEGME Copolymer. To fabricate the resistive water level sensor based on the AgNWs/PEDOT:PSS-*g*-PEGME hybrid film, AgNWs were spin coated on the PET film at 60 °C and dried at 120 °C for 2 min. This coating process of AgNWs was repeated once. DMSO (5 wt %), PEGME (PSS/PEGME weight ratio = 1:0.5) and capstone fs-30 (0.2 wt %) were added to the PEDOT:PSS solution. The mixture was stirred for over 1 h at room temperature (25 °C) before being spin coated through a 0.45 μm PVDF syringe filter on the PET film at 1500 rpm for 60 s and thermally annealed at 120 °C for 15 min in air. Finally, the AgNWs/PEDOT:PSS-*g*-PEGME hybrid film was patterned using an

https://doi.org/10.1021/acsomega.2c00017
ACS Omega 2022, 7, 15459−15466

infrared (IR) laser (laser irradiation wavelength = 1054 nm) to fabricate the resistive water level sensor.

Characterization and Measurements of the Water Level Sensor. To characterize and measure the resistive water level sensor, X-ray photoelectron spectroscopy (XPS, Thermo UK, K-alpha) was performed to analyze the elemental composition of the AgNWs/PEDOT:PSS-*g*-PEGME hybrid film before and after IR laser irradiation. The transmittance and surface morphology were measured using an ultraviolet−visible−near-infrared (UV−vis−NIR) spectrophotometer (Agilent, Cary 5000) and SEM (JEOL JSM-6710F), respectively. The thickness of the AgNWs/PEDOT:PSS-*g*-PEGME hybrid film was measured using atomic force microscopy. Electrical characterization of the resistive water level sensor was performed using a Keithley 4200-Semiconductor Characterization System.

■ ASSOCIATED CONTENT

Supporting Information

The Supporting Information is available free of charge at https://pubs.acs.org/doi/10.1021/acsomega.2c00017.

EDX analysis of AgNWs/PEDOT:PSS-*g*-PEGME hybrid film on PET before and after IR laser irradiation, relative atomic concentrations of AgNWs/PEDOT:PSS-*g*-PEGME hybrid film on PET before and after IR laser irradiation (PDF)

■ AUTHOR INFORMATION

Corresponding Authors

Seongin Hong − *Department of Physics, Gachon University, Seongnam 13120, Republic of Korea;* orcid.org/0000-0002-7056-5467; Email: seongin@gachon.ac.kr

Sunkook Kim − *School of Advanced Materials Science & Engineering, Sungkyunkwan University, Suwon 440-745, Republic of Korea;* orcid.org/0000-0003-1747-4539; Email: seonkuk@skku.edu

Authors

Seungho Baek − *School of Advanced Materials Science & Engineering, Sungkyunkwan University, Suwon 440-745, Republic of Korea*

Jung Joon Lee − *School of Advanced Materials Science & Engineering, Sungkyunkwan University, Suwon 440-745, Republic of Korea;* orcid.org/0000-0003-0835-7381

Jonghwan Shin − *School of Advanced Materials Science & Engineering, Sungkyunkwan University, Suwon 440-745, Republic of Korea*

Jung Ho Kim − *Institute for Superconducting and Electronic Materials, Australian Institute for Innovative Materials, University of Wollongong, North Wollongong 2500 New South Wales, Australia*

Complete contact information is available at: https://pubs.acs.org/10.1021/acsomega.2c00017

Author Contributions

#S.B. and J.J.L. contributed equally.

Notes

The authors declare no competing financial interest.

■ ACKNOWLEDGMENTS

This research was supported by the Basic Science Research Program through the National Research Foundation of Korea (NRF) funded by the Ministry of Education (2020R1I1A1A01070907, 2020R1I1A1A01073884). This work was supported by Institute of Information & communications Technology Planning & Evaluation (IITP) grant funded by the Korea government (MSIT) (No. 2021-0-01151). This work was partly supported by the GRRC program of Gyeonggi province [GRRC Sungkyunkwan 2017-B06, Nano-biosensor based on flexible material]. This work was supported by "Human Resources Program in Energy Technology" of the Korea Institute of Energy Technology Evaluation and Planning (KETEP), granted financial resource from the Ministry of Trade, Industry & Energy, Republic of Korea.(No.20214000000590). Public domain images used in Figure 1 and the TOC and Abstract graphics were from the following sources: PNG EGG (wifi icon), Pixabay (sky), CRD Center (grass), Free3D (plant), Unsplash (hand holding phone).

■ ABBREVIATIONS

EDX, energy-dispersive X-ray; InSAR, interferometric synthetic aperture radar; IoT, Internet of Things; SEM, scanning electron microscopy; XPS, X-ray photoelectron spectroscopy

■ REFERENCES

(1) Gubbi, J.; Buyya, R.; Marusic, S.; Palaniswami, M. Internet of Things (IoT): A Vision, Architectural Elements, and Future Directions. *Futur. Gener. Comput. Syst.* **2013**, *29* (7), 1645−1660.

(2) Stankovic, J. A. Research Directions for the Internet of Things. *IEEE Internet Things J.* **2014**, *1* (1), 3−9.

(3) Cai, X.; Geng, S.; Wu, D.; Cai, J.; Chen, J. A Multicloud-Model-Based Many-Objective Intelligent Algorithm for Efficient Task Scheduling in Internet of Things. *IEEE Internet Things J.* **2021**, *8* (12), 9645−9653.

(4) Muangprathub, J.; Boonnam, N.; Kajornkasirat, S.; Lekbangpong, N.; Wanichsombat, A.; Nillaor, P. IoT and Agriculture Data Analysis for Smart Farm. *Comput. Electron. Agric.* **2019**, *156*, 467−474.

(5) Ayaz, M.; Ammad-Uddin, M.; Sharif, Z.; Mansour, A.; Aggoune, E. H. M. Internet-of-Things (IoT)-Based Smart Agriculture: Toward Making the Fields Talk. *IEEE Access* **2019**, *7*, 129551−129583.

(6) Fan, J.; Zhang, Y.; Wen, W.; Gu, S.; Lu, X.; Guo, X. The Future of Internet of Things in Agriculture: Plant High-Throughput Phenotypic Platform. *J. Clean. Prod.* **2021**, *280*, 123651.

(7) Khan, F. A.; Ibrahim, A. A.; Zeki, A. M. Environmental Monitoring and Disease Detection of Plants in Smart Greenhouse Using Internet of Things. *J. Phys. Commun.* **2020**, *4* (5), 055008.

(8) Giraldo, J. P.; Wu, H.; Newkirk, G. M.; Kruss, S. Nanobiotechnology Approaches for Engineering Smart Plant Sensors. *Nat. Nanotechnol.* **2019**, *14* (6), 541−553.

(9) Alahi, M. E. E.; Xie, L.; Mukhopadhyay, S.; Burkitt, L. A Temperature Compensated Smart Nitrate-Sensor for Agricultural Industry. *IEEE Trans. Ind. Electron.* **2017**, *64* (9), 7333−7341.

(10) Lu, Y.; Xu, K.; Zhang, L.; Deguchi, M.; Shishido, H.; Arie, T.; Pan, R.; Hayashi, A.; Shen, L.; Akita, S.; Takei, K. Multimodal Plant Healthcare Flexible Sensor System. *ACS Nano* **2020**, *14* (9), 10966−10975.

(11) Lee, K.; Park, J.; Lee, M. S.; Kim, J.; Hyun, B. G.; Kang, D. J.; Na, K.; Lee, C. Y.; Bien, F.; Park, J. U. In-Situ Synthesis of Carbon Nanotube-Graphite Electronic Devices and Their Integrations onto Surfaces of Live Plants and Insects. *Nano Lett.* **2014**, *14* (5), 2647−2654.

(12) Rocchi, A.; Santecchia, E.; Barucca, G.; Mengucci, P. Optimization of Distances Measurement by an Ultrasonic Sensor. *Mater. Today Proc.* **2019**, *19* (8), 33−39.

(13) Wang, Z.; Yu, Y.; Wang, Y.; Lu, X.; Cheng, T.; Bao, G.; Wang, Z. L. Magnetic Flap-Type Difunctional Sensor for Detecting

Pneumatic Flow and Liquid Level Based on Triboelectric Nanogenerator. *ACS Nano* **2020**, *14* (5), 5981−5987.
(14) Hong, S. H.; Wdowinski, S.; Kim, S. W.; Won, J. S. Multi-Temporal Monitoring of Wetland Water Levels in the Florida Everglades Using Interferometric Synthetic Aperture Radar (InSAR). *Remote Sens. Environ.* **2010**, *114* (11), 2436−2447.
(15) Hong, S.; Lee, J. J.; Gandla, S.; Park, J.; Cho, H.; Kim, S. Resistive Water Sensors Based on PEDOT:PSS- g-PEGME Copolymer and Laser Treatment for Water Ingress Monitoring Systems. *ACS Sensors* **2019**, *4* (12), 3291−3297.
(16) Huseynova, G.; Hyun Kim, Y.; Lee, J. H.; Lee, J. Rising Advancements in the Application of PEDOT:PSS as a Prosperous Transparent and Flexible Electrode Material for Solution-Processed Organic Electronics. *J. Inf. Dispersion* **2020**, *21* (2), 71−91.
(17) Lee, J. J.; Gandla, S.; Lim, B.; Kang, S.; Kim, S.; Lee, S.; Kim, S. Alcohol-Based Highly Conductive Polymer for Conformal Nanocoatings on Hydrophobic Surfaces toward a Highly Sensitive and Stable Pressure Sensor. *NPG Asia Mater.* **2020**, *12* (1), 65.
(18) Lee, J. J.; Yoo, D.; Park, C.; Choi, H. H.; Kim, J. H. All Organic-Based Solar Cell and Thermoelectric Generator Hybrid Device System Using Highly Conductive PEDOT:PSS Film as Organic Thermoelectric Generator. *Sol. Energy* **2016**, *134*, 479−483.
(19) Won, Y.; Lee, J. J.; Shin, J.; Lee, M.; Kim, S.; Gandla, S. Biocompatible, Transparent, and High-Areal-Coverage Kirigami PEDOT:PSS Electrodes for Electrooculography-Derived Human-Machine Interactions. *ACS Sensors* **2021**, *6* (3), 967−975.
(20) Gueye, M. N.; Carella, A.; Faure-Vincent, J.; Demadrille, R.; Simonato, J. P. Progress in Understanding Structure and Transport Properties of PEDOT-Based Materials: A Critical Review. *Prog. Mater. Sci.* **2020**, *108*, 100616.
(21) Lee, J. J.; Lee, S. H.; Kim, F. S.; Choi, H. H.; Kim, J. H. Simultaneous Enhancement of the Efficiency and Stability of Organic Solar Cells Using PEDOT:PSS Grafted with a PEGME Buffer Layer. *Org. Electron.* **2015**, *26*, 191−199.
(22) Wang, T.; Lu, K.; Xu, Z.; Lin, Z.; Ning, H.; Qiu, T.; Yang, Z.; Zheng, H.; Yao, R.; Peng, J. Recent Developments in Flexible Transparent Electrode. *Crystals* **2021**, *11* (5), 511.
(23) Cho, W.; Hong, J. K.; Lee, J. J.; Kim, S.; Kim, S.; Im, S.; Yoo, D.; Kim, J. H. Synthesis of Conductive and Transparent PEDOT:P-(SS-Co-PEGMA) with Excellent Water-, Weather-, and Chemical-Stabilities for Organic Solar Cells. *RSC Adv.* **2016**, *6* (68), 63296−63303.
(24) Abdel Rehim, M. H.; Youssef, A. M.; Al-Said, H.; Turky, G.; Abouly, M. Polyaniline and Modified Titanate Nanowires Layer-by-Layer Plastic Electrode for Flexible Electronic Device Applications. *RSC Adv.* **2016**, *6* (97), 94556−94563.
(25) Heo, S. Y.; Choi, H. J.; Park, B. J.; Um, J. H.; Jung, H. J.; Jeong, J. R.; Yoon, S. G. Effect of Protective Layer on Enhanced Transmittance, Mechanical Durability, Anti-Fingerprint, and Antibacterial Activity of the Silver Nanoparticles Deposited on Flexible Substrate. *Sensors Actuators, A Phys.* **2015**, *221*, 131−138.
(26) Yoo, D.; Son, W.; Kim, S.; Lee, J. J.; Lee, S. H.; Choi, H. H.; Kim, J. H. Gradual Thickness-Dependent Enhancement of the Thermoelectric Properties of PEDOT:PSS Nanofilms. *RSC Adv.* **2014**, *4* (103), 58924−58929.
(27) Mengistie, D. A.; Ibrahem, M. A.; Wang, P. C.; Chu, C. W. Highly Conductive PEDOT:PSS Treated with Formic Acid for ITO-Free Polymer Solar Cells. *ACS Appl. Mater. Interfaces* **2014**, *6* (4), 2292−2299.

https://doi.org/10.1021/acsomega.2c00017
ACS Omega 2022, 7, 15459−15466